Distinct element method for multiscale modeling of cross-linked carbon nanotube bundles: From soft to strong nanomaterials

Igor Ostanin
Department of Civil Engineering, University of Minnesota, Minneapolis, Minnesota 55455, USA

Roberto Ballarini
Department of Civil and Environmental Engineering, University of Houston, Houston, Texas 77204, USA

Traian Dumitrică[a)]
Department of Mechanical Engineering, University of Minnesota, Minneapolis, Minnesota 55455, USA; and Department of Civil Engineering, University of Minnesota, Minneapolis, Minnesota 55455, USA

(Received 28 May 2014; accepted 18 August 2014)

Predicting the impact of cross-links on the mechanics of carbon nanotube-based materials is a challenging endeavor, as the micro- and nanostructure is composed of continuous nanofibers, discontinuous interfaces, and covalent bridges. Here we demonstrate a new modeling solution in the context of the distinct element method (DEM). By representing nanotubes as bonded cylinder segments undergoing van der Waals adhesion, viscous friction, and contact bonding, we are able to simulate how cross-linking transforms a soft bundle into a strong one. We predict that the sp^3-sp cross-links formed by interstitial carbon atoms can improve the tensile strength by an order of magnitude, in agreement with experiment and molecular dynamics simulations. The DEM methodology allows performing the multiscale simulation needed for developing strategies to further enhance the mechanical performance.

I. INTRODUCTION

Since their discovery, carbon nanotubes[1] (CNTs) have attracted significant interest in applications, especially because of their extraordinary mechanical properties.[2–7] These properties include Young's modulus close to 1 TPa,[8] and over 150 GPa and 16% yield stress[5] and strains,[4] respectively. Assemblies of CNTs, such as freestanding and supported films,[9] yarns,[10] and fibers,[11,12] have been accomplished to extend the characteristic properties of a single CNT in the macroscopic scale. However, mechanical properties of such structures are inferior compared to those of individual CNTs. The reason these CNT assemblies belong to the category of soft nanomaterials is the poor load transfer by the van der Waals (vdW) interaction between CNTs.[7] Various strategies are currently being pursued to overcome this problem, including the covalent bridging of CNTs introduced by irradiation methods[13–16] and the mechanical interlocking.[17] In this respect, an order of magnitude in the moduli and tensile strengths of irradiated CNT bundles have been already reported.[18]

While much of the current work is directed at modeling the outcomes of irradiation on the CNT structure and mechanical properties, and at understanding the microscopic details of the cross-links,[19,20] it remains unclear how one can leverage this knowledge to predict the global mechanical behavior of a CNT bundle. Molecular dynamics (MD) has been applied to model the mechanics of cross-linked CNTs.[21,22] It has been shown that cross-links can dramatically enhance the intertube shear.[23] However, simulation times and system size constraints limit the predictive capabilities of this approach to CNT bundles. To establish a connection with the mechanical-testing experiments, a multiscale simulation methodology is needed.[24,25] While large-scale mechanical behavior of materials is usually treated with continuum mechanics, simulation of noncontinuous phenomena, like the anticipated gliding of CNTs against each other, is not well adapted to a continuous description. Giving maximum priority to realism, we propose here to apply the recently developed distinct element method (DEM) for CNTs,[26,27] because this approach naturally takes into account discontinuities, and also can be connected to the microscopic description of matter.

DEM, the macroscopic method introduced by Cundall and Strack[28] more than 30 years ago, is currently used for simulating the mechanical properties of geological materials and structures. We have found this method to be natural for CNTs, which have macroscopic persistence lengths and whose mechanics is not sensitive to temperature.[29] In prior works,[26,27] we have adapted DEM at the mesoscale[26] to simulate the mechanics of CNTs. Each CNT is represented by a chain of rigid cylindrical

[a)]Address all correspondence to this author.
e-mail: dtraian@umn.edu
This author was an editor of this focus issue during the review and decision stage. For the *JMR* policy on review and publication of manuscripts authored by editors, please refer to http://www.mrs.org/jmr-editor-manuscripts/.
DOI: 10.1557/jmr.2014.279

 © Materials Research Society 2015

https://doi.org/10.1557/jmr.2014.279 Published online by Cambridge University Press

elements interacting with each other via contact models informed by simulations we performed at the atomistic scale.[30–32] References 27 and 33 give detailed descriptions of how these microscopic interactions are incorporated into specific contact models. Below we only outline the basic model and describe its new extension to include cross-linking.

II. DEM FOR CARBON NANOTUBES WITH CROSS-LINKS

We consider here bundles formed with (10,10) CNTs of length $L_{CNT} = 67.8$ nm. A CNT is represented by fifty distinct elements. Each element, lumping 220 C atoms, is characterized by its mass and inertia, taken here the inertia tensor of a 3.35 Å thick hollow cylinder with dimensions matching the CNT portion it represents. The translational motion of each element is described with the velocity Verlet scheme, while the rotational motion is treated with a 4th order Runge–Kutta method, combined with quaternion representation of rotations.[34] Neighboring distinct elements representing a CNT interact through standard parallel bonds that capture the linear elasticity of the CNT walls. Physically, the parallel bonds can be viewed as rings of distributed springs located at the interface of elements. These bonds resist stretching, shearing, bending, and torsional deformations. The normal and shear stiffness parameters of the parallel bonds are found from atomistic data. The microscopic vdW interaction between CNT segments is included with vdW contacts derived by us. Note that our vdW contact model captures the short-range anisotropy of the interaction between cylindrical segments, and thus provides realistic shear interactions between CNTs. Two channels of energy dissipation are present: (i) a local damping, which is used solely to stabilize time integration, and (ii) a physically meaningful viscous damping, which acts in parallel with the vdW contact model and aims at capturing the energy dissipation occurring during intertube sliding. The viscous damping coefficient D was calibrated[33] to reproduce the mechanical behavior observed in experiments.

In prior works[33,35] we used the DEM framework summarized above to investigate the mechanics of aligned CNTs interacting solely via vdW forces. Our simulations demonstrated the importance of viscous damping in reaching a representative response. In agreement with experiment, we found that the sliding of the tubes against one another severely limits the strength and elastic moduli of the representatively long and thick CNT fibers. This behavior contrasts with what would be obtained by employing the usual isotropic treatment of the vdW interactions between coarse-grained elements. The isotropic treatment leads to staggering-induced corrugation,[26,27] an artifact that prevents the sliding of individual CNTs within the mechanically deformed fiber. Thus, the existing DEM model for CNT represents a suitable basis for building a multiscale model for the problem at hand.

At this juncture, we introduce new contact bonds to explicitly represent the mechanics of the cross-links between CNTs. These added bonds between face-to-face distinct elements already in vdW contact support only compressive and shear loadings. In our rather qualitative study reported here, we apply this approach to describe the type of cross-links formed by one interstitial C atom covalently bonded with two CNT surfaces. These sp^3-sp links are relevant experimentally and well characterized microscopically.[20] The simple DEM contact model is appropriate because mechanically such a cross-link represents a breakable elastic spring.

Considering that the kinematics of the problem resolves only the sliding of the CNTs, which causes shear relative motion of the bonded face-to-face segments, the shear stiffness of the contact bond is calibrated to represent the elasticity of the cross-link. In Fig. 1 we describe the calibration procedure. Assuming that at the vdW equilibrium interspacing $l_0 = 3.35$ Å the initial links are unstrained, the elastic behavior of the microscopic cross-link is incorporated into the shear force-displacement law of the contact bond. The critical elongation of the shear contact spring is $\Delta x = \sqrt{(1+\varepsilon_c)^2 l_0^2 - l_0^2} = 3.75$ Å. Based on the interatomic dependence of the classical potentials for carbon,[36] we infer that the cross-link can sustain a $\varepsilon_c = 0.5$ critical strain before it breaks. The shear stiffness of the DEM contact bond is found by equating at Δx the strain energy of the contact shear spring with the microscopic energy of two single covalent bonds $2E_b$, where $E_b = 3.6$ eV.[36] It follows that $k_s = 4E_b/(\Delta x)^2 = 1.02\,\text{eV/Å}^2$. The strength of the DEM shear spring is $f_c = k_s \Delta x = 3.82$ eV/Å

III. CNT BUNDLE ASSEMBLY AND MECHANICAL TEST SETUP

Our simulations considered close-packed bundle of CNTs with a hexagonal cross-section. The side of a hexagon is $(N-1)r_0$, where $N = 3$ is the number of tubes along the side and $r_0 = 17.1$ Å is the center-to-center distance between the constituent CNTs. The number of CNTs that define the bundle cross-section is $1 + 3N(N-1)$ while the cross-sectional area of the bundle is given by $S = 0.75\sqrt{3}[1 + 3N(N-1)]r_0^2$. The simulated bundle has a length L of 271.2 nm comprising $M = 4$ individual CNTs. In a row of CNTs there is no spacing between the CNT caps and so distinct elements of each row of CNTs face the elements of neighboring rows. A number of cross-linking contact bonds presented are then distributed in a random manner over the volume

https://doi.org/10.1557/jmr.2014.279 Published online by Cambridge University Press

of the bundle. The number of vdW contacts in the bundle is $N_{\mathrm{vdw}} = 800\left[3 + 9(N-1)^2\right] = 31{,}200$. We denote by γ the ratio between the number of cross-linked elements and face-to-face vdW contacts.

In preparation for the simulation, the bundle is allowed to relax for 10,000 cycles, or 0.1 ns. We observe that the bundle contracts along the x-direction, leading to approximately 0.3% decrease in length and a decrease in elastic strain energy of 0.5 kJ/kg. Bundles may also develop lateral deformations, and store part of the elastic energy in bending. This behavior is due to the inherent asymmetry introduced by the randomly positioned cross-links. After the relaxation process is completed, two layers of distinct elements located at both ends of the bundle are designated as grip elements. The x degree of freedom of the grip elements are kept fixed, and the bundle is equilibrated for an additional 1000 cycles (0.01 ns), to ensure that the initial force acting on each grip is zero. A displacement-controlled loading is next achieved by accelerating the grip elements from 0 to the given velocity during 5000 cycles (0.05 ns). A stress–strain curve is recorded during the simulations. The tensile stress is defined as $\sigma_{xx} = F_x/S$, where F_x is the x-component of the force acting on the grip. A nominal strain is defined as $\varepsilon_{xx} = 2u_x^{\mathrm{g}}/L$, where u_x^{g} is the x-component of the grip displacement.

To examine the sliding of the CNTs during the tensile load, we have computed for each distinct element i its slip vector $\vec{\delta}^i$, defined as

$$\vec{\delta}^i = \frac{1}{\lambda_i}\sum_{j=1}^{\lambda_i}\left(\vec{X}^{(ij)} - \vec{x}^{(ij)}\right) \quad . \tag{1}$$

Here $\vec{x}^{(ij)}$ and $\vec{X}^{(ij)}$ are the vector differences between the coordinates of elements i and j in the current and initial states, respectively, and λ_i is the number of nearest-neighbor elements for i in the initial reference configuration. We have also monitored the energy balance during the quasistatic tension tests, given by

$$A_{\mathrm{ext}}(\varepsilon) = \Delta U_{\mathrm{pot}}(\varepsilon) + \Delta Q(\varepsilon) \quad . \tag{2}$$

Here $A_{\mathrm{ext}}(\Delta)$ is the work done by the external load. ΔU_{pot} is the change in the total potential energy of the bundle comprising ΔU_{str} the change in the strain energy of individual CNTs; $\Delta U_{\mathrm{bonds}}$, the elastic energy stored in the cross-links; and ΔU_{vdw}, the change in the vdW adhesion energy associated with the formation of new vdW surfaces; and ΔQ, the energy dissipated by local and viscous damping.

IV. RESULTS AND DISCUSSION

We first focus on understanding the mechanical response. The evolving force-chain network, shown in Fig. 2, governs the complex response of the CNT bundle to the applied tensile load. In all of the considered CNT bundles with three representative densities of cross-linking (with γ being 0, 0.1, and 0.2), the individual CNTs provide stable force chain portions for carrying the applied tensile load. Although the vdW contacts between CNTs, some of which are filled with cross-links, undergo massive breakages, they are still able to ensure load transfer between individual CNTs for the entire duration of the tensile tests. (Note that in Fig. 2 the breaking of the vdW bonds is not represented.) Additionally, in Figs. 2(b) and 2(c), it can be seen that more and more cross-links are breaking under the increasing applied strain, leading to the formation of nanoscale-localized fracture zones.

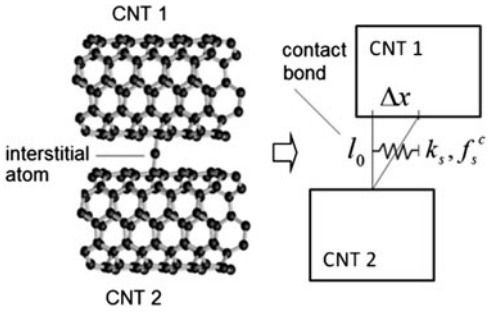


FIG. 1. The elasticity and strength of a microscopic sp^3-sp link between two CNTs is represented in DEM via the shear strength and stiffness values of the contact bond between distinct elements located on the two CNTs.

More insight emerges from Fig. 3, which displays the slip vector magnitude and energy components. On one hand, the CNT of the pristine bundle, Fig. 3(a) exhibits significant sliding even at the incipient stages of the deformation. The force chains passing through the CNTs carry little load, as it can be seen in the evolution of the strain energy component. The CNT sliding causes significant growth of the vdW and dissipation energy components. On the other hand, the presence of cross-links successfully inhibits the CNT sliding, Figs. 3(b) and 3(c), and the strain energy stored in the CNTs and cross-links dominates at the small strain levels. The work done by external forces practically equals the change in potential energy. Next, the $\gamma = 0.1$ (0.2) bundle under 2% (3%) applied strain starts to develop localized sliding in zones which coincide with the cross-link fracture areas identified in Fig. 2. Beyond these strain levels, the elastic energy stored in the bundle starts to exhibit a significant decrease, as the cross-link fracture zones increase in size. Post-peak deformation is associated with massive energy dissipation into the microscopic degrees of freedom. Using a CNT heat capacity value of 710 J/(kg K) we estimate an increase of the $\gamma = 0.2$ bundle temperature by 120 K.

We now focus on the stress/strain relationship displayed by the CNT bundles. Each curve of Fig. 4

https://doi.org/10.1557/jmr.2014.279 Published online by Cambridge University Press

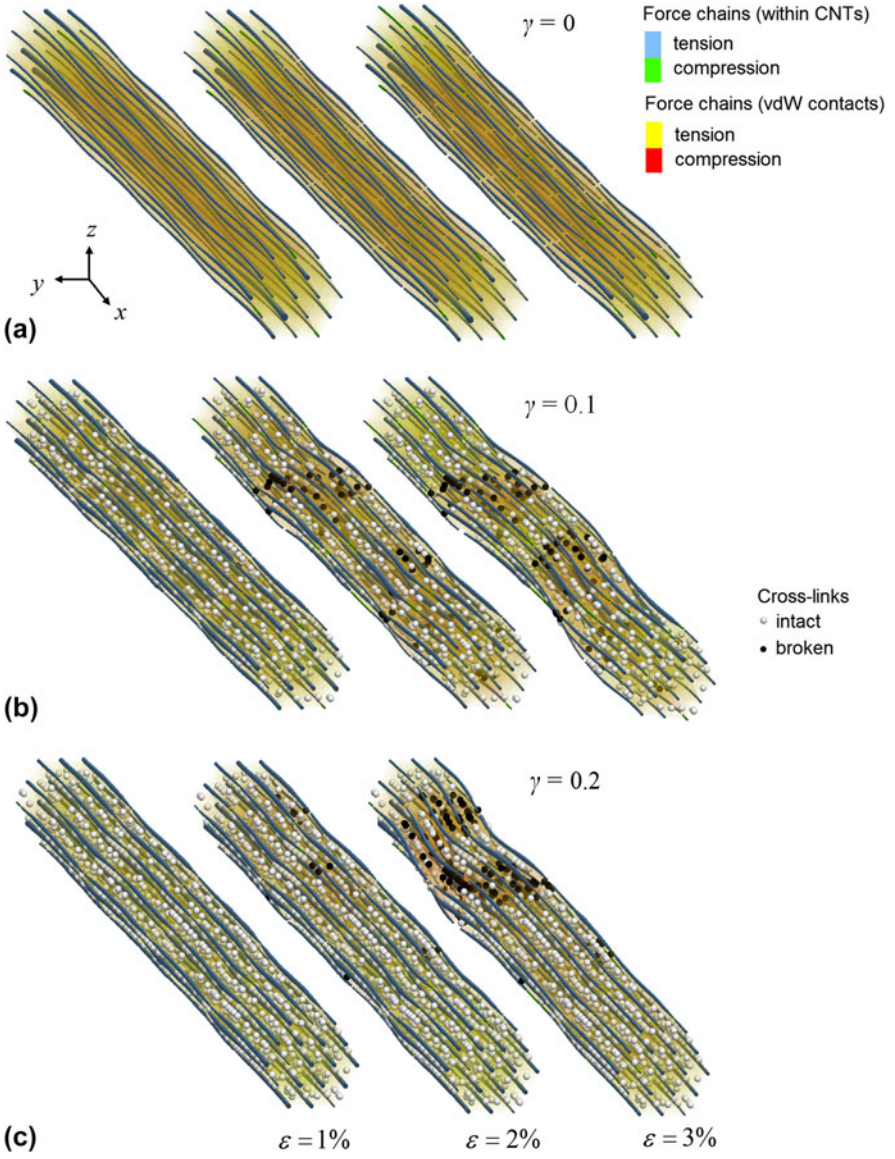


FIG. 2. CNT bundle at different strain levels, showing force chains as cylinders with the thickness dependent on the magnitude of normal force. Tension and compression within CNTs are in blue and green respectively. Load transfer through vdW forces is visualized with semitransparent cylinders, yellow in tension and red in compression. Also visible are the distributions of the interstitial atoms containing intact (white) and broken (black) cross-links. The tensile tests considered bundles with three cross-link densities: (a) $\gamma = 0$, (b) $\gamma = 0.1$, and (c) $\gamma = 0.2$.

starts with a linear regime of loading (characterized by the Young's modulus E), followed by the yield, which occurs at the peak value of stress σ_c and corresponding strain ε_c. The computational results presented in Fig. 4(a) show that the stress–strain curves are very sensitive to cross-linking. The values of E, σ_c, and ε_c, summarized in Table I, demonstrate a significant improvement in the mechanical properties with the cross-link density. In particular, we predict that cross-linking can improve the strength by an order of magnitude.

It is instructive to compare the values reported in Table I with the ones of an ideal bundle containing a similar hexagonal arrangement of CNTs each of length L. To perform this comparison, we rescaled the ideal CNT Young's modulus and tensile strengths by the ratio $(S_c/S_t) = 2.6$. Here, S_t and S_c are the cross-sectional area of the (10,10) CNT and the cross-sectional area occupied by the (10,10) CNT in a hexagonal bundle, respectively. We obtained an ideal Young's modulus of 385 GPa and strength of 56 GPa. As can be seen from Table I, the computed elastic moduli are approaching the ideal value. The smaller-than-ideal values for the bundles are caused by the compliance of the cross-links. However, the bundle peak stress and strains are still inferior to the ideal CNT yield values.

https://doi.org/10.1557/jmr.2014.279 Published online by Cambridge University Press

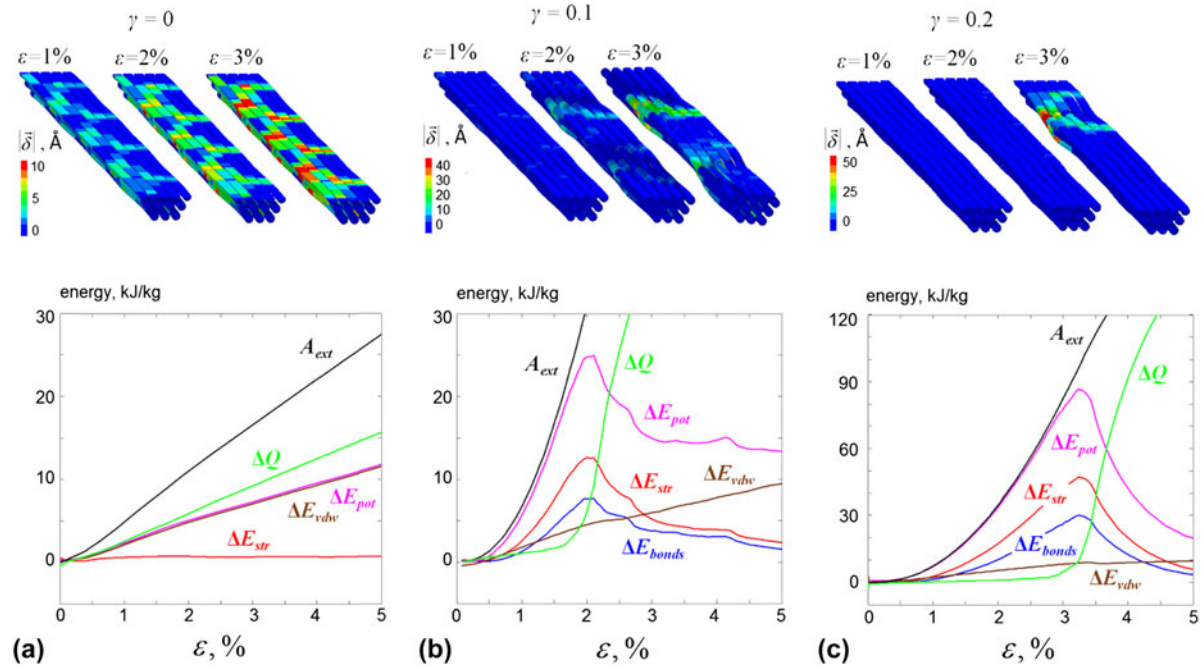


FIG. 3. Bundle axial cross-section showing the slip vector magnitude (above) and energy components (below) during tensile tests carried out with three cross-link densities: (a) $\gamma = 0$, (b) $\gamma = 0.1$, and (c) $\gamma = 0.2$.

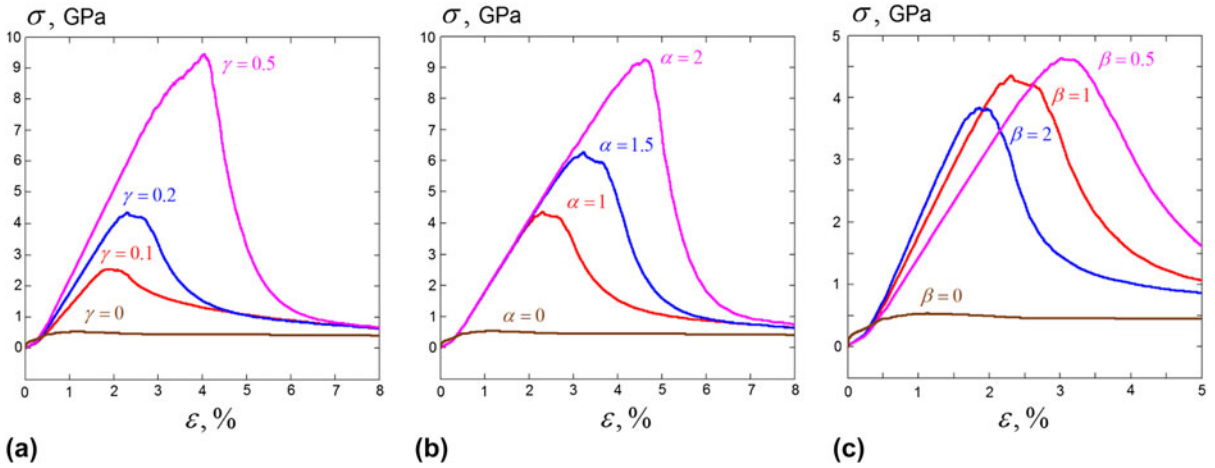


FIG. 4. Stress–strain curves obtained by DEM simulation showing the dependence on the cross-links' (a) density, (b) strength, and (c) stiffness. In (b) and (c) $\gamma = 0.2$.

We have performed additional investigations to explore the impact of the strength and stiffness of the cross-link on the overall mechanical response. Figures 4(b) and 4(c) summarize our simulation results in which the cross-link DEM contact bond strength and stiffness values were multiplied by the dimensionless parameters α and β, respectively. From these simulations, we learn that a brittle response is favored by populating the CNT bundle with strong and stiff bonds. A ductile behavior can instead be achieved by introducing weak and compliant bonds. Stiffer bonds give rise to higher Young's moduli, as can be seen from the slopes of the initial linear variations shown in Fig. 4(c). To achieve large σ_c and ε_c values, a combination of strong and compliant cross-links is required. The latter requirement

TABLE I. Variations of the Young's modulus, critical strain, and stress with the cross-link density.

γ	E (GPa)	σ_c (GPa)	ε_c (%)
0.0	49.29	0.53	1.12
0.1	129.48	2.55	1.84
0.2	169.26	4.34	2.29
0.5	210.80	9.45	4.03

https://doi.org/10.1557/jmr.2014.279 Published online by Cambridge University Press

can be explained with the fact that compliant cross-links resolve significant relative slip of CNTs within the bundle, which leads to the formation of a new vdW surface and participation of vdW surface tension forces in the response.

Our DEM simulations are consistent with the full molecular dynamic simulations considering the same type of cross-linking in crystalline bundles made up of (5,5) CNTs.[22] These bundles with dense cross-links demonstrated Young's moduli on the order of 50 GPa and a fracture strain of 8%. To compare the strength, we have to first account for the difference in cross-sectional areas between (10,10) and (5,5) CNT bundles. On this basis, we extrapolate the MD value of the strength for (10,10) CNTs to be ~18 GPa. These results are consistent with our DEM tests and can be captured with cross-links of comparable density and double strength ($\alpha = 2$). The factor of two in strength obtained in MD can be explained by the fact that interstitial atoms formed more than one single covalent bond with atoms on the CNT surfaces.

V. CONCLUSION

We developed a successful DEM representation for CNTs, by mapping the microscopic mechanics onto cylindrical distinct elements forming parallel contact bonds and vdW bonds with viscous damping. The DEM methodology was used to investigate the mechanics of a variety of CNT assemblies, including CNT films, rings, rackets, and bundles.[27,33,35,37] Here, we enriched this framework by extending the interactions between the distinct elements to include covalent sp^3-sp links between CNTs. Our simulations provide a detailed mesoscale picture of the complex mechanical response of the CNT bundles with various cross-link densities, and capture the transformation of the bundle from a soft into a strong material. The DEM simulations presented here show good agreement with MD simulations and experiment[18] in all the important aspects and offer possible strategies for the further engineering of the stress–strain curve.

We emphasize that with the exception of viscous damping (shown to play a less important role – see the supplementary material), all other parameters of our model were obtained from microscopic data. We used DEM in a multiscale manner, to formulate "hands-off" predictions based on microscopic data. Neither complex global constitutive models nor assumptions about the location and type of yield are imposed a priori to simulate the mechanical response. By informing the contact models employed here with new data, our DEM approach can be readily used to investigate the impact on the mechanical response of other important cross-links.[16] Another effect that deserves further exploration is the influence of a cross-link distribution on the strength of the bundle.[20] Indeed, in practice the uniform distribution considered here is relevant for thin bundles only. For thicker bundles, the presence of cross-links is limited to the regions around the surface of the bundle. It was observed that increasing the dosage of irradiation improves the penetration and thus yields cross-links toward the middle of the bundle. However, the procedure also produces detrimental effects on the CNT structure, such as vacancy-related defects.[38] The mechanical weakening of the individual CNT due to irradiation could also be captured by the parameterization of the DEM parallel contact bonds.

ACKNOWLEDGMENTS

We thank the Itasca Consulting Group for the PFC3D software support. I.O. and T.D. acknowledge the support of the NSF through CMMI 1332228.

REFERENCES

1. S. Iijima: Helical microtubules of graphite carbon. *Nature* **354**, 56 (1991).
2. A. Krishnan, E. Dujardin, T.W. Ebbesen, P.N. Yianilos, and M.M.J. Treacy: Young's modulus of single-walled nanotubes. *Phys. Rev. B* **58**, 14013 (1998).
3. T. Dumitrică, T. Belytschko, and B.I. Yakobson: Bond-breaking bifurcation states in carbon nanotube fracture. *J. Chem. Phys.* **118** (21), 9485 (2003).
4. T. Dumitrică, M. Hua, and B.I. Yakobson: Symmetry-, time-, and temperature-dependent strength of carbon nanotubes. *Proc. Natl. Acad. Sci. U.S.A.* **103**(18), 6105 (2006).
5. B.G. Demczyk, Y.M. Wang, J. Cumings, M. Hetman, W. Han, A. Zettl, and R.O. Ritchie: Direct mechanical measurement of the tensile strength and elastic modulus of multiwalled carbon nanotubes. *Mater. Sci. Eng., A* **334**, 173 (2002).
6. M.F. Yu, O. Lourie, M.J. Deyer, K. Moloni, T.F. Kelly, and R.S. Ruoff: Strength and breaking mechanism of multiwalled carbon nanotubes under tensile load. *Science* **287**, 637 (2000).
7. J-P. Salvetat, G.A.D. Briggs, J-M. Bonard, R.R. Bacsa, A.J. Kulik, T. Stöckli, N.A. Burnham, and L. Forró: Elastic and shear moduli of single-walled carbon nanotube ropes. *Phys. Rev. Lett.* **82**, 944 (1999).
8. M-F. Yu, B.S. Files, S. Arepalli, and R.S. Ruoff: Tensile loading of ropes of single wall carbon nanotubes and their mechanical properties. *Phys. Rev. Lett.* **84**, 5552 (2000).
9. J.M. Harris, G.R.S. Iyer, A.K. Bernhardt, J.Y. Huh, S.D. Hudson, J.A. Fagan, and E.K. Hobbie: Electronic durability of flexible transparent films from type-specific single-wall carbon nanotubes. *ACS Nano* **6**, 881 (2012).
10. J. Foroughi, G.M. Spinks, G.G. Wallace, J. Oh, M.E. Kozlov, S. Fang, T. Mirfakhrai, J.D.W. Madden, M.K. Shin, S.J. Kim, and R.H. Baughman: Torsional carbon nanotube artificial muscles. *Science* **334**, 494 (2011).
11. A.B. Dalton, S. Collins, E. Muñoz, J.M. Razal, V.H. Ebron, J.P. Ferraris, J.N. Coleman, B.G. Kim, and R.H. Baughman: Super-tough carbon-nanotube fibres. *Nature* **423**, 703 (2003).

https://doi.org/10.1557/jmr.2014.279 Published online by Cambridge University Press

12. Y-L. Li, I.A. Kinloch, and A.H. Windle: Direct spinning of carbon nanotube fibers from chemical vapor deposition synthesis. *Science* **304**, 276 (2004).
13. A.V. Krasheninnikov and F. Banhart: Engineering of nanostructured carbon materials with electron or ion beams. *Nat. Mater.* **6**, 723 (2007).
14. A. Kis, G. Csányi, J.P. Salvetat, T.N. Lee, E. Couteau, A.J. Kulik, W. Benoit, J. Brugger, and L. Forró: Reinforcement of single-walled carbon nanotube bundles by intertube bridging. *Nat. Mater.* **3**, 153 (2004).
15. T. Filleter and H.D. Espinosa: Multi-scale mechanical improvement produced in carbon nanotube fibers by irradiation cross-linking. *Carbon* **56**, 1 (2013).
16. N.P. O'Brien, M.A. McCarthy, and W.A. Curtin: Improved inter-tube coupling in CNT bundles through carbon ion irradiation. *Carbon* **51**, 173 (2013).
17. A de Juan, Y. Pouillon, L. Ruiz-González, A. Torres-Pardo, S. Casado, N. Martín, Á. Rubio, and E.M. Pérez: Mechanically interlocked single-wall carbon nanotubes. *Angew. Chem., Int. Ed.* **53**, 5394 (2014).
18. T. Filleter, R. Bernal, S. Li, and H.D. Espinosa: Ultrahigh strength and stiffness in cross-linked hierarchical carbon nanotube bundles. *Adv. Mater.* **23**, 2855 (2011).
19. A.V. Krasheninnikov and K. Nordlund: Ion and electron irradiation-induced effects in nanostructured materials. *J. Appl. Phys.* **107**, 071301 (2010).
20. N.P. O'Brien, M.A. McCarthy, and W.A. Curtin: A theoretical quantification of the possible improvement in the mechanical properties of carbon nanotube bundles by carbon ion irradiation. *Carbon* **53**, 346 (2013).
21. B. Ni, R. Andrews, D. Jacques, D. Qian, M.B.J. Wijesundara, Y.S. Choi, and S.B. Sinnott: A combined computational and experimental study of ion-beam modification of carbon nanotube bundles. *J. Phys. Chem. B* **105**, 12719 (2001).
22. C.F. Cornwell and C.R. Welch: Very-high-strength (60-GPa) carbon nanotube fiber design based on molecular dynamics simulations. *J. Chem. Phys.* **134**, 204708 (2011).
23. Z.H. Xia, P.R. Guduru, and W.A. Curtin: Enhancing mechanical properties of multiwall carbon nanotubes via sp(3) interwall bridging. *Phys. Rev. Lett.* **98**, 245501 (2007).
24. L. Zhigilei, C. Wei, and D. Srivastava: Mesoscopic model for dynamic simulations of carbon nanotubes. *Phys. Rev. B* **71**, 165417 (2005).
25. M. Buehler, Y. Kong, and H. Gao: Deformation mechanisms of very long single-wall carbon nanotubes subject to compressive loading. *J. Eng. Mater. Technol.* **126**, 245 (2004).
26. T. Anderson, E. Akatyeva, I. Nikiforov, D. Potyondy, R. Ballarini, and T. Dumitrică: Toward distinct element method simulations of carbon nanotube systems. *J. Nanotechnol. Eng. Med.* **1**, 041009 (2010).
27. I. Ostanin, R. Ballarini, D. Potyondy, and T. Dumitrică: A distinct element method for large scale simulations of carbon nanotube assemblies. *J. Mech. Phys. Solids* **61**, 762 (2013).
28. P.A. Cundall and O.D.L. Strack: A discrete model for granular assemblies. *Geotechnique* **29**(1), 47 (1979).
29. M. Xu, D.N. Futaba, T. Yamada, M. Yumura, and K. Hata: Carbon nanotubes with temperature-invariant viscoelasticity from -196 to 1000°C. *Science* **330**, 1364 (2010).
30. I. Nikiforov, D-B. Zhang, R.D. James, and T. Dumitrică: Wavelike rippling in multi-walled carbon nanotubes under pure bending. *Appl. Phys. Lett.* **96**, 123107 (2010).
31. D-B. Zhang and T. Dumitrică: Elasticity of ideal single-walled carbon nanotubes via symmetry-adapted tight-binding objective modeling. *Appl. Phys. Lett.* **93**, 031919 (2008).
32. A. Carlson and T. Dumitrică: Extended tight-binding potential for modeling intertube interactions in carbon nanotubes. *Nanotechnology* **18**, 065706 (2007).
33. I. Ostanin, R. Ballarini, and T. Dumitrică: Distinct element method modeling of carbon nanotube bundles with intertube sliding and dissipation. *J. Appl. Mech.* **81**, 061004 (2014).
34. S.M. Johnson, J.R. Williams, and B.K. Cook: Quaternion-based rigid body rotation integration algorithms for use in particle methods. *Int. J. Numer. Methods Eng.* **74**, 1303 (2008).
35. Y. Wang, M. Semler, I. Ostanin, E.K. Hobbie, and T. Dumitrică: Rings and rackets from single-wall carbon nanotubes: Manifestations of mesoscale mechanics. *Soft Matter* (2014). DOI: 10.1039/C4SM00865K.
36. J. Tersoff: New empirical approach for the structure and energy of covalent systems. *Phys. Rev. B* **37**, 6991 (1988).
37. Y. Wang, C. Gaidau, I. Ostanin, and T. Dumitrică: Ring windings from single-wall carbon nanotubes: A distinct element method study. *Appl. Phys. Lett.* **103**, 183902 (2013).
38. Z. Osváth, G. Vértesy, L. Tapasztó, F. Wéber, Z.E. Horváth, J. Gyulai, and L.P. Biró: Atomically resolved STM images of carbon nanotube defects produced by Ar+ irradiation. *Phys. Rev. B* **72**, 045429 (2005).

Supplementary Material

To view the supplementary material for this article, please visit http://dx.doi.org/jmr.2014.279.

https://doi.org/10.1557/jmr.2014.279 Published online by Cambridge University Press